RSC Advances

ROYAL SOCIETY OF CHEMISTRY

www.rsc.org/advances

Journal Name

RSCPublishing

COMMUNICATION

Improved performance in flexible organic solar cells via optimization of highly transparent silver grid/graphene electrodes

Cite this: DOI: 10.1039/x0xx00000x

Received ooth January 2012,
Accepted ooth January 2012

DOI: 10.1039/x0xx00000x

www.rsc.org/

Myoung Joo Cha,[1,2] Sung Man Kim,[3] Seong Jun Kang,[3] Jung Hwa Seo,[1,*] and Bright Walker[2,*]

Organic solar cells (OSCs) were fabricated on polyethylene terephthalate (PET) substrates using hybrid silver grid/graphene films as transparent conducting electrodes and the effect of silver grid dimensions was characterized. OSCs fabricated using optimized grid dimensions of 200 µm× 200 µ m × 50 nm × 2 µm (length × width × height × linewidth) on PET substrates exhibited two times the power conversion efficiency of control devices using graphene only.

Organic solar cells (OSCs) are attractive optoelectronic devices due to their low processing cost, large area, light weight and superior flexibility.[1-4] Many flexible OSCs have been demonstrated using flexible transparent electrodes such as metal nanowires,[5,6] conducting polymers,[7,8] carbon nanotubes (CNT)[9,10] and graphene[11-13,] since the commonly used material indium-tin oxide (ITO) is deficient in flexible applications due to poor mechanical properties and corrosion of the ITO by poly(3,4-ethylenedioxythiophene) polystyrene sulfonate (PEDOT:PSS).[14]

Among transparent conducting materials, graphene is particularly attractive as a next generation transparent electrode due to its high transmittance of ~97%, superior electrical conductivity, mechanical properties and good flexibility.[15-18] In addition, graphene can be used for both anodes and cathodes by controlling its work function using metal nanoparticles or molecular dopants.[19] Many researchers have studied graphene transparent conducting films as replacements for ITO electrodes in optoelectronic devices. For example, Gomez de Arco *et al.* reported that OSCs using graphene (as the anode) deposited by chemical vapor deposition (CVD), which exhibited a power conversion efficiency (PCE) of 1.18%.[20] Cox *et al.* fabricated OSCs using single layer graphene (SLG) as a cathode having a PCE of 0.24%.[21] The devices reported so far have exhibited low PCEs compared to OSCs using ITO electrodes, due to the high sheet resistance of graphene. Therefore it is critical to reduce the sheet resistance of graphene in order to realize high device performance with flexible transparent electrodes.

Hybrid electrodes based on graphene have progressed via the use of metal grids to improve the electrical conductivity of graphene.[22-24] Some reports show that graphene with metal grids has superior optical and electrical properties as well as improved flexibility.[22,23] To further enhance the conductivity of the PEDOT anode in polymer solar cells, Aernouts *et al.* applied a metallic Ag grid to PEDOT:PSS, and Glatthaar *et al.* reported an inverted cell using a PEDOT anode with thermally deposited Au lines.[25,26] More recently, Tvingstedt *et al.* demonstrated the possibility of replacing ITO in OSCs using an anode comprising PEDOT and metallic micro-Ag-grids, which were formed using a soft-lithography metal-deposition method.[27] It is of particular interest that hybrid metal grid / graphene electrodes can be easily deposited by roll-to-roll processes such as nanoimprinting or inkjet printing, which makes them highly amenable to large scale mass production compared to conventional ITO films.[28-30] Our previous report showed that multilayer graphene (MLG) with a silver grid on a glass substrate had optical transmittance of ~85%, a sheet resistance of 28 Ω/square and yielded a PCE of 2.38%, in conjunction with a poly 3-hexylthiophene active layer, which was similar to the PCE of control devices using ITO.[25]

Despite the good properties of hybrid films, studies regarding the effects of grid dimensions on the optoelectronic properties of transparent electrodes are few. However, grid dimensions constitute a critical parameter which must be optimized in order to achieve high optical transmittance and low sheet resistance using hybrid films, as the characteristics of hybrid films strongly depend on the grid geometry and graphene thickness. When the grid linewidth is

increased, the sheet resistance of the hybrid films is improved. However, the transmittance is decreased due to the opacity of the metal grid. Since the transmittance of the hybrid films depends on the grid geometry, further studies on graphene/metal grid hybrid films are needed to achieve high performance in optoelectronic devices.

In this work, we have studied the effect of silver grid size on the properties of transparent anodes using polyethylene terephthalate (PET) substrates and investigated their application in photovoltaic devices. To in order to optimize the properties of the transparent anodes, optical transmittance and sheet resistance were measured using UV-Vis and 4-point probe measurements, respectively. Flexible OSCs were fabricated using a bulk heterojunction (BHJ) architecture consisting of poly(3-hexylthiophere):[6,6]-phenyl C_{71} butyric acid methyl ester ($P_3HT:PC_{71}BM$) as the active layer and device characteristics were correlated to the metal grid sizes.

Silver grids were formed on PET substrates using a conventional photolithography process and lift-off method. The silver grids were 50-nm thick and were deposited onto positive photoresist patterned PET substrates by thermal evaporation. Graphene layers were grown on copper foil by chemical vapour deposition (CVD) and polymethylmethacrylate (PMMA, 950K PMMA C4) was spin coated onto the graphene/Cu foil as a supporting layer. After etching the Cu foil using a Ni etchant, graphene was transferred onto Ag grid/PET substrates. The SLG hybrid films with silver grids were then completed by removing the PMMA using acetone. Field emission scanning electron microscopy (FESEM) (LEO SUPRA 55, Carl Zeiss) was used to characterize the structure of the hybrid films (not shown here). Optical transmittance was measured using a UV/Vis spectrometer (V-570, JASCO) and sheet resistance was measured using the 4-point probe method.

Conventional OSCs were fabricated using hybrid transparent SLG/Ag grid films, as shown Fig. 1(a). A detailed schematic of the device structure is illustrated in Fig. 1(b). Before making the devices, the SLG/Ag grid surfaces were treated under UV-ozone for 5 min to modify the surface energy. PEDOT:PSS from Heraeus which has 10 ~ 100 S/cm conductivity was then spin coated (as a hole transport layer) onto the SLG/Ag grid films and annealed at 140 °C for 10 minutes, resulting in a film thickness of ~40 nm. Organic active layers comprising $P_3HT:PC_{71}BM$ were then deposited; a blend solution (1:1) of P3HT and $PC_{71}BM$ in dichlorobenzene was spin coated and annealed at 60 °C for 30 min. The resulting thickness of $P_3HT:PC_{71}BM$ layer was 100 nm. Next, an ultra-thin (> 5 nm) conjugated polyelectrolyte (CPE) layer was deposited as an electron extraction layer. The CPE poly[9,9-bis[6′-(N,N,N-trimethylammonium)hexyl]fluorene-altco-1,4-phenylene] tetrakis (imidazoly) borate ($PFN^+BIm_4^-$),[31] was deposited onto the $P_3HT:PC_{71}BM$ surface from a dilute solution in methanol by spin coating at 2000 rpm for 40 s. Finally, Al (70nm) cathodes were thermally evaporated through a shadow mask defining an active area of 0.09 cm^2. Devices were characterized under ambient conditions using simulated AM1.5G irradiation (100 mW/cm^2), which was calibrated with a standard silicon photodiode. Reported device characteristics represent the average of 10 devices. Standard deviations for PCEs were found to be less than 0.3%.

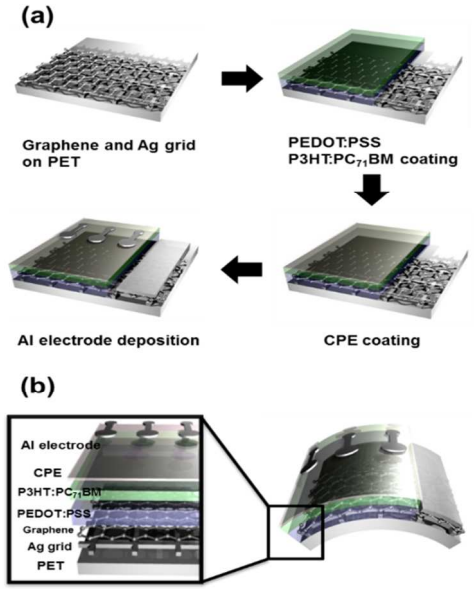

FIG 1. (a) Schematic diagram of OSCs using hybrid transparent anodes. (b) Illustration of the device structure with Ag grids under SLG films.

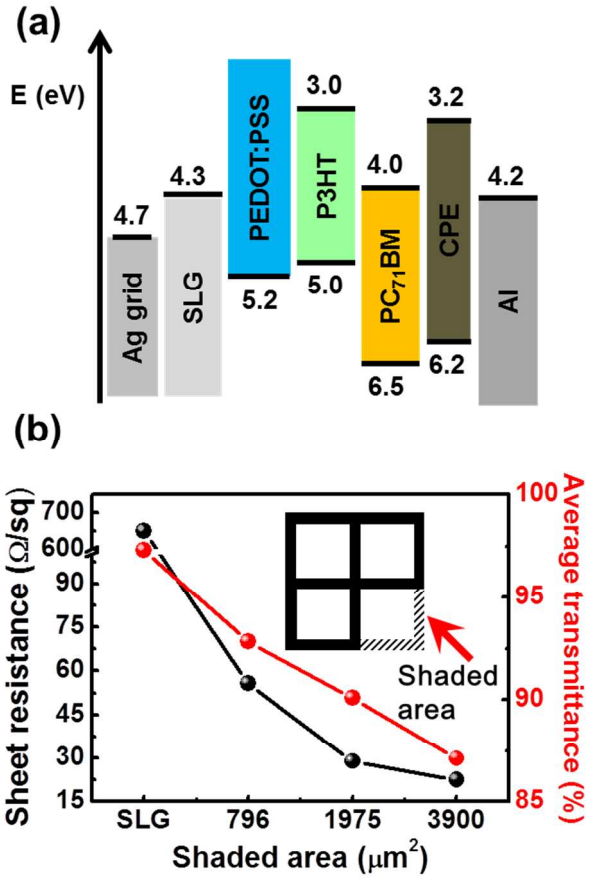

FIG 2. (a) Energy band diagram of OSCs with hybrid transparent anodes. (b) Sheet resistance and transmittance versus shaded area. Shaded area was calculated; 200 × 2 × 50 to 796 μm^2, 200 × 5 × 50 to 1975 μm^2, and 200 × 10 × 50 to 3900 μm^2. The inset is a schematic of the shaded area used in this study.

Figure 2(a) shows an energy band diagram of the OSCs. The work functions of Ag grid and SLG are 4.7 and 4.3 eV, respectively; where the work function of SLG was obtained by ultraviolet photoelectron spectroscopy.[32] The highest occupied molecular orbital (HOMO) and the lowest unoccupied molecular orbital (LUMO) levels of PEDOT:PSS, P3HT, $PC_{71}BM$, and CPE were taken from the literature.[25,33] The CPE layer functioned as an electron extraction layer via the formation of an interfacial dipole.[31] According to the energy band diagram, the hybrid SLG films exhibit similar work functions, which are comparable to the work function of conventional ITO anodes.[34] Figure 2(b) shows the optical transmittance and sheet resistances of SLG and SLG/Ag for various grid sizes. SLG films show an average transparency of 97% at 550 nm; the transmittance is fairly constant across the visible spectrum regardless of wavelength.[35] However, SLG films exhibit a relatively high sheet resistance of 650 Ω/sq. The high sheet resistance of the SLG films is a disadvantage for their applications in optoelectronic devices. The hybrid conductive SLG/Ag grid films exhibit a fairly constant transparency of 85 ~ 92% over a wide spectral range between 500 and 850 nm, while the sheet resistance of SLG/Ag grid films decreases dramatically to 14 ~ 56 Ω/sq using Ag grids. In the previous study, the average surface roughness obtained from the dimensions of the grids was approximately 2.47 nm, since haziness is generally related to the rough films.[24] Thus, we can expect good haze properties and minimal light scattering due to the carefully controlled dimensions of mesh and the small surface coverage of Ag.

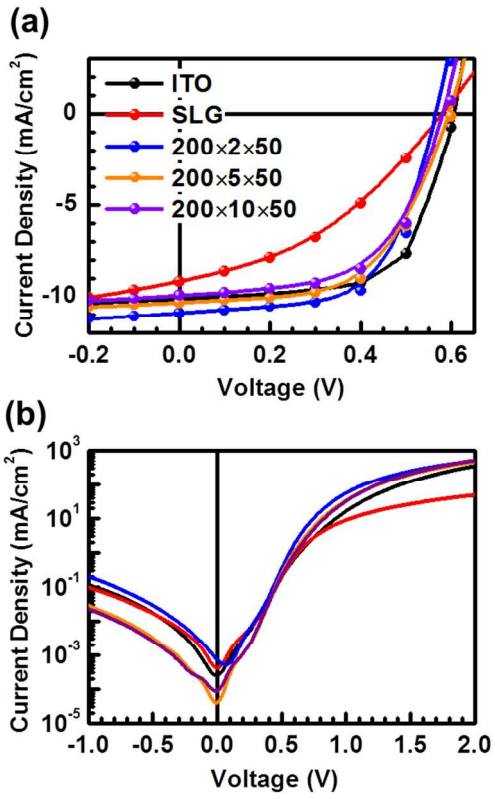

FIG 3. J-V characteristics of P3HT:$PC_{71}BM$ devices using ITO anodes as control devices (black), PET/SLG anodes (red) and PET/various Ag grid size/SLG anodes (blue, orange and purple) (a) under illumination and (b) dark.

Table 1. Performance of BHJ devices with ITO substrates and graphene substrates as a function of Ag grid size

	J_{SC} (mA/cm²)	V_{OC} (V)	FF (%)	PCE (Best)	PCE (average)	R_{SH} (kΩ)	R_S (Ω)
ITO	10.1	0.60	62.4	3.8	3.6	93.5	41.0
SLG	9.2	0.58	38.0	2.0	1.8	113.3	298.2
200 × 2 × 50	10.9	0.58	60.8	3.9	3.8	55.5	27.3
200 × 5 × 50	10.3	0.60	57.9	3.6	3.3	409.8	29.4
200 × 10 × 50	9.9	0.60	57.4	3.4	3.1	507.6	26.7

Figure 3 shows the current density–voltage (J-V) characteristics of P3HT:$PC_{71}BM$ solar cells using Ag grids with dimensions (length × width × height × linewidth) including 200 μm × 200 μm × 50 nm × 2 μm, 200 μm × 200 μm × 50 nm × 5 μm and 200 μm × 200 μm × 50 nm × 10 μm sizes. Two types of control devices based on ITO and PET/SLG substrates were also prepared. Table 1 summarizes the performance of different devices. The first control device using an ITO substrate exhibited a short circuit current (J_{SC}) of 10.1 mA/cm², open circuit voltage (V_{OC}) of 0.60 V and fill factor (FF) of 62.4%, resulting in a PCE of 3.8%. Despite the advantages of flexible substrates, the performance of devices using PET/graphene substrates was inferior to devices using ITO substrates. The difference in PCEs for devices using ITO and PET/SLG substrates can be attributed to SLG having a lower work function (4.3 eV) than ITO (4.7 eV), causing a mismatch with the valence band energy of PEDOT:PSS (5.2 eV); this results in an energy barrier for hole transfer from the PEDOT:PSS layer to the graphene electrode. Additionally, PET/SLG substrates have a much larger sheet resistance than ITO. Similar to the ITO substrate, devices using PET/Ag grid/SLG substrates yielded PCEs in range of 3.4 ~ 3.9%, with an optimal performance of 3.9% including a J_{SC} of 10.9 mA/cm², V_{OC} of 0.58 V and FF of 60.8%, when the 200 μm × 200 μm × 50 nm × 2 μm Ag grid size was used. Notably, the FF was increased from 55% to 61% upon incorporation of the Ag grid. The V_{OC} remained almost unchanged, while J_{SC} and FF values increased (9.2 mA/cm² to 10.9 mA/cm² and 38% to 61%, respectively). The PCE increased from 2.0% to 3.9%; an enhancement of about 90%. This large change in performance via the introduction of Ag grid is attributed to low sheet resistance and an increase in work function. The sheet resistance of SLG anode decreased by more than an order of magnitude from 650 Ω/sq, to 22 ~ 55 Ω/sq upon incorporation of Ag grids. The J-V characteristics of the devices measured in the dark are shown in Fig 3(b). In the regime from -1 to 0 V, the leakage current of SLG device (red line) and 200 μm × 200 μm × 50 nm × 2 μm (blue line) are not greatly changed compared to the ITO devices (black line). However, the presence of 200 μm × 200 μm × 50 nm × 5 μm (orange line) and 200 μm × 200 μm × 50 nm × 10 μm (purple line) Ag grids reduced leakage current and increased shunt resistance (R_{SH}) (93.5, 409.8, and 507.6 KΩ for ITO, 200 μm × 200 μm × 50 nm × 5 μm , and 200 μm × 200 μm × 50 nm × 10 μm Ag grid, respectively). In the regime from 0 V

to 0.7 V, the curves of ITO and SLG devices are almost identical to those of hybrid Ag grid/SLG devices, which is consistent with the constant V_{OC} observed for all devices. For the case of V > 0.7 V, the series resistance (R_S) of the SLG was 298.2 Ω, and the devices with various size Ag grid exhibited R_S values of 27.3 Ω for 200 μm × 200 μm × 50 nm × 2 μm, 29.4 Ω for 200 μm × 200 μm × 50 nm × 5 μm and 26.7 Ω for 200 μm × 200 μm × 50 nm × 10 μm, respectively. Thus, the performance of devices incorporating Ag grid was improved via increased R_{SH} and decreased R_S.

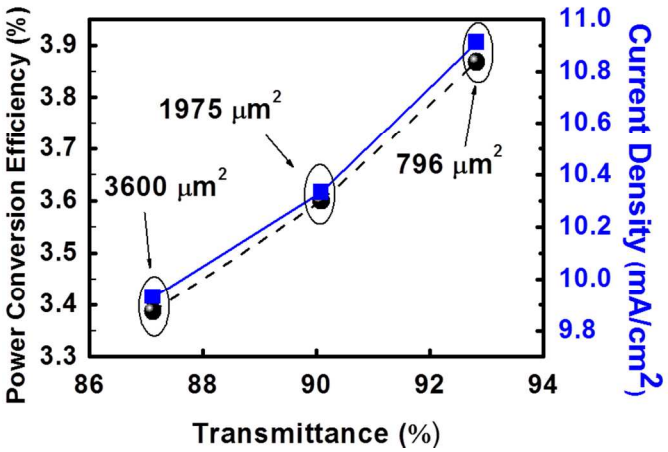

FIG 4. Current density and power conversion efficiency versus transmittance.

Figure 4 shows the current density and PCE versus transmittance of substrates for different shaded area. The photovoltaic performance is strongly correlated to the transmittance of the substrates. The grid spacing of 200 μm × 200 μm yields an open area 0.040 mm^2; using Ag line widths of 2 μm, 5 μm and 10 μm results in shaded areas of 796 μ m^2, 1975 $μm^2$ and 3900 $μm^2$ in each grid cell, respectively, which are able to transmit light. The transmittance of device with 796 $μm^2$ shaded area was 92.83 %, and decreased with increasing shaded area. This decrease in transmittance closely tracked with a decrease in J_{SC}. The high transmittance of our composite electrodes explains the high PCE compared to the reference ITO-based solar cells, since more light is transmitted to the absorber layer, more charge carries are generated and extracted. We suggest that the strategy presented here constitutes a useful approach to improving the performance of OSCs based on graphene transparent electrodes.

Conclusions

Hybrid transparent conducting films were fabricated using graphene synthesized by CVD coupled with Ag grids deposited via a transfer process. The SLG films show a high sheet resistance (650 Ω/sq) and a high optical transmittance (97% at 550 nm), while the hybrid Ag/SLG films exhibited reduced sheet resistances (14 ~ 56 Ω/sq) and optical transmittance (85 ~ 92%). The hybrid transparent SLG films were employed as anodes in P3HT:PC_{71}BM solar cell, yielding a J_{SC} of 9.2 mA/cm^2, V_{OC} of 0.58 V, FF of 38.0%, and a PCE of 2.0%. OSCs using SLG/Ag grid anodes exhibited enhanced performance compared to devices with only SLG films. A 91 % improvement in PCE compared to devices using SLG films alone was observed. These results demonstrate that hybrid SLG/Ag grid films are a suitable transparent electrode for use in optoelectronic applications and constitute a promising route to improve the performance of OSCs based on graphene electrodes, for large area and low-cost solar cell manufacture.

Acknowledgements

This work was supported by the National Research Foundation of Korea (NRF-2013R1A1A2011591, NRF-2013R1A1A1A05007934 and NRF-2014R1A1A1037729). This work was supported by the Center for Advanced Soft-Electronics funded by the Ministry of Science, ICT and Future Planning as a Global Frontier Project (CASE-2014M3A6A5060946).

Notes and references

[1] Department of Materials Physics, Dong-A University, Busan 604-714, Republic of Korea
[2] School of Energy and Chemical Engineering, Ulsan National Institute of Science and Technology, Ulsan, 689-798, Republic of Korea
[3] Department of Advanced Materials Engineering for Information and Electronics, Kyung Hee University, Yongin, 446-701, Republic of Korea

1 F. C. Krebs, *Sol. Energy Mater. Sol. Cells.*, 2009, **93**, 394.
2 C. J. Brabec, S. Gowrisanker, J. J. M. Halls, D. Laird, S. Jia, and S. P. Williams, *Adv. Mater.*, 2010, **22**, 3839.
3 H.-Y. Chen, J. Hou, S. Zhang, Y. Liang, G. Yang, Y. Yang, Y. Wu, L. Yu, Y. Wu and G. Li, *Nat. Photonics.*, 2009, **3**, 649.
4 Z. Yin, S. Sun, T. Salim, S. Wu, X. Huang, Q. He, Y. M. Lam, and H. Zhang, *ACS Nano*, 2010, **4**, 5263.
5 J. Y. Lee, S. T. Connor, Y. Cui, and P. Peumans, *Nano Lett.*, 2008, **8**, 689.
6 M. G. Kang, T. Xu, H. J. Park, X. Luo, and L. J. Guo, *Adv. Mater.*, 2010, **22**, 4378.
7 S. -I. Na, S. -S. Kim, J. Jo and D. -Y. Kim, *Adv. Mater.*, 2008, **20**, 4061.
8 J. Zou, H. -L. Yip, S. K. Hau, and A. K. Y. Jen, *Appl. Phys. Lett.*, 2010, **96**, 203301.
9 M. W. Rowell, M. A. Topinka, M. D. McGehee, H. J. Prall, G. Dennler, N. S. Sariciftci, L. Hu, and G. Gruner, *Appl. Phys. Lett.*, 2006, **88**, 233506.
10 R. C. Tenent, T. M. Barnes, J. D. Bergeson, A. J. Ferguson, B. To, L. M. Gedvulas, M. J. Heben, and J. L. Blackburn *Adv. Mater.*, 2009, **21**, 3210.
11 X. Wan, G. Long, L. Huang, and Y. Chen, *Adv. Mater.*, 2011, **23**, 5342.
12 Y Choi, S. J. Kang, H. Kim, W. M. Choi, S. Na, *Sol. Energy Mater. Sol. Cells.*, 2012, **96**, 281.
13 H. Park, P. R. Brown, V. Bulovic, and Jing Kong, *Nano Lett.*, 2012, **12**, 133.
14 Y. Suh, N. Lu, S. H. Lee, W. –S. Chung, K. Kim, B. Kim, M. J. Ko, and M. J. Kim, *Appl. Mater. Interface*, 2012, **4**, 5118.
15 J. K. Wassei and R. B. Kaner, *Mater. Today*, 2010, **13**, 52.
16 C. Lee, X. Wei, J. W. Kysar, and J. Hone, *Science*, 2008, **321**, 385.

17 X. Li, Y. Zhu, W. Cai, M. Borysiak, B. Han, D. Chen, R. D. Piner, L. Colombo and R. S. Ruoff, *Nano Lett.*, 2009, **9**, 4359.
18 K. S. Kim, Y. Zhao, H. Jang, S. Y. Lee, J. M. Kim, K. S. Kim, J. H. Ahn, P. Kim, J. Y. Choi, and B. H. Hong, *Nature*, 2009, **457**, 706.
19 Y. Shi, K. K. Kim, A. Reina, M. Hofmann, L. –J. Li, and J. Kong, *ACS Nano*, 2010, **4**, 2689.
20 L. G. De Arco, Y. Zhang, C. W. schlenker, K. Ryu, M. E. Thompson, and C. Zhou, *ACS Nano*, 2010, **4**, 2865.
21 M. Cox, A. Gorodetsky, B. Kim, K. S. Kim, Z. Jia, P. Kim, C. Nuckolls, and L. Kymissis, *Appl. Phys. Lett.*, 2011, **98**, 123303.
22 Y. Zhu, Z. Sun, Z. Yan, Z. Jin and J. M. Tour, *ACS Nano*, 2011, **8**, 6472.
23 S. M. Kim, and S. J. Kang, *J. Korean Phys. Soc.*, 2014, **64**, 177.
24 S. M. Kim, B. Walker, J. H. Seo, and S. J. Kang, *Jpn. J. Appl. Phys.*, 2013, **52**, 125103.
25 T. Aernouts, P. Vanlaeke, W. Geens, J. Poortmans, P. Heremans, S. Borghs, R. Mertens, R. Andriessen, and L. Leenders, *Thin Solid films*, 2004, **22**, 451.
26 M. Glatthaar, M. Niggemann, B. Zimmermann, P. Lewer, M. Riede, A. Hinsch, and J. Luther, *Thin Solid films*, 2005, **491**, 298.
27 K. Tvingstedt, and O. Inganas, *Adv. Mater.*, 2007, **19**, 2893.
28. J.-S. Yu, I. Kim, J.-S. Kim, J. Jo, T. T. Larsen-Olsen, R. R. Søndergaard, M. Hösel, D. Angmo, M. Jørgensen and F. C. Krebs, *Nanoscale*, 2012, **4**, 6032.
29. K. Ellmer, *Nat. Photonics*, 2012, **6**, 809.
30. S. Bae, H. Kim, Y. Lee, X. Xu, J.-S. Park, Y. Zheng, J. Balakrishnan, T. Lei, H. Ri Kim, Y. I. Song, Y.-J. Kim, K. S. Kim, B. Özyilmaz, J.-H. Ahn, B. H. Hong and S. Iijima, *Nat. Nanotechnol*., 2010, **5**, 574.
31 B. Walker, A. Tamayo, J. Yang, J. Z. Brzezinski, and T. –Q. Nguyen, *Appl. Phys. Lett.*, 2008, **93**, 063302.
32 A. Siokou, F. Ravani, S. Karakalos, O. Frank, M. Kalbac, and C. Galiotis, *Appl. Surf. Sci.*, 2011, **257**, 9785.
33 B. A. Collins, Z. Li, R. Tumbleston, E. Gann, C. R. McNeill, and H. Ade, *Adv. Energy Mater.*, 2013, **3**, 65.
34 Y. Wang, S. W. Tong, X. F. Xu, B. Ozyilmaz, and K. P. Loh, *Adv. Mater.*, 2011, **23**, 1514
35 H. Kim, S. H. Bae, T. H. Han, K. G. Lim, J.-H. Ahn and T. W. Lee, *Nanotechnology*, 2014, **25**, 014012

Organic solar cells were fabricated on polyethylene terephthalate (PET) substrates using hybrid silver grid/graphene films as transparent conducting electrodes and the effect of silver grid dimensions was characterized.